Composite mesostructures by nano-confinement

YIYING WU[1], GUOSHENG CHENG[1], KIRILL KATSOV[2], SCOTT W. SIDES[3], JIANFANG WANG[1], JING TANG[2], GLENN H. FREDRICKSON[2,3], MARTIN MOSKOVITS[1] AND GALEN D. STUCKY[1,2]*

[1]Department of Chemistry and Biochemistry, University of California, Santa Barbara, California 93106, USA
[2]Materials Research Laboratory, University of California, Santa Barbara, California 93106, USA
[3]Department of Chemical Engineering, University of California, Santa Barbara, California 93106, USA
*e-mail: stucky@chem.ucsb.edu

Published online: 17 October 2004; doi:10.1038/nmat1230

In a physically confined environment, interfacial interactions, symmetry breaking, structural frustration and confinement-induced entropy loss can play dominant roles in determining molecular organization. Here we present a systematic study of the confined assembly of silica–surfactant composite mesostructures within cylindrical nanochannels of varying diameters. Using exactly the same precursors and reaction conditions that form the two-dimensional hexagonal SBA-15 mesostructured thin film, unprecedented silica mesostructures with chiral mesopores such as single- and double-helical geometries spontaneously form inside individual alumina nanochannels. On tightening the degree of confinement, a transition is observed in the mesopore morphology from a coiled cylindrical to a spherical cage-like geometry. Self-consistent field calculations carried out to account for the observed mesostructures accord well with experiment. The mesostructures produced by confined syntheses are useful as templates for fabricating highly ordered mesostructured nanowires and nanowire arrays.

Previously reported studies of confinement effects[1–4] have centred on block copolymers, especially the bulk lamella-forming block-copolymer assembly in one-dimensional (1D) confinement. For example, for symmetric diblock-copolymer film sandwiched between two flat surfaces, when the film thickness is incommensurate with the natural lamella periodicity, deviation from natural periodicity occurs[3]. Cylindrical channels represent an interesting 2D confining environment, in which lamella-forming block copolymer forms a concentric multilayered cylindrical mesophase provided that the wall surface preferentially interacts with one polymer block[5]. The systematic definition of periodic structure as a function of cylindrical confinement for either organic or composite systems remains to be determined. Here we describe the morphogeneses of new mesostructured materials that arise on fine-tuning the physical confining environment for co-assembly of silica and block copolymer.

Non-ionic poly(alkylene oxide) block copolymers have been widely used as surfactants for synthesizing highly ordered silica–surfactant composite mesostructures as a result of inorganic–organic cooperative assembly[6]. Hexagonal silica mesostructures (SBA-15), for example, have been synthesized in the presence of triblock poly(ethylene oxide)–poly(propylene oxide)–poly(ethylene oxide) (PEO–PPO–PEO) copolymers[7]. The ethylene oxide/propylene oxide ratio of the copolymer moieties can be used to tune the formation of various mesophases with lamellar, hexagonal or cubic symmetries. These silica mesostructured and mesoporous materials have wide applications as catalyst hosts[8], molecule-separation membranes[9] and optical materials[10].

In this work, we systematically studied the confined assembly of silica–copolymer composite mesostructures within cylinders of varying diameters. We used nanochannels electrochemically created in porous anodic alumina (PAA) membranes[11] to physically confine the synthesis of mesostructured silica. The nanochannels, with diameters systematically varied from 18 nm to 80 nm, were loaded with mesostructured silica using the sol–gel dip-coating method[12–15]. The dip-coating precursor solution, which was the same in every instance, was prepared by mixing tetraethyl orthosilicate (TEOS), poly(ethylene oxide)-*b*-poly(propylene oxide)-*b*-poly(ethylene oxide) block copolymer $EO_{20}PO_{70}EO_{20}$ (Pluronic P123), diluted hydrochloric acid (pH 2) and ethanol, with a molar ratio of 1 TEOS: 0.0096 P123: 6 H_2O: 8.8 ethanol: 0.001 HCl, as described

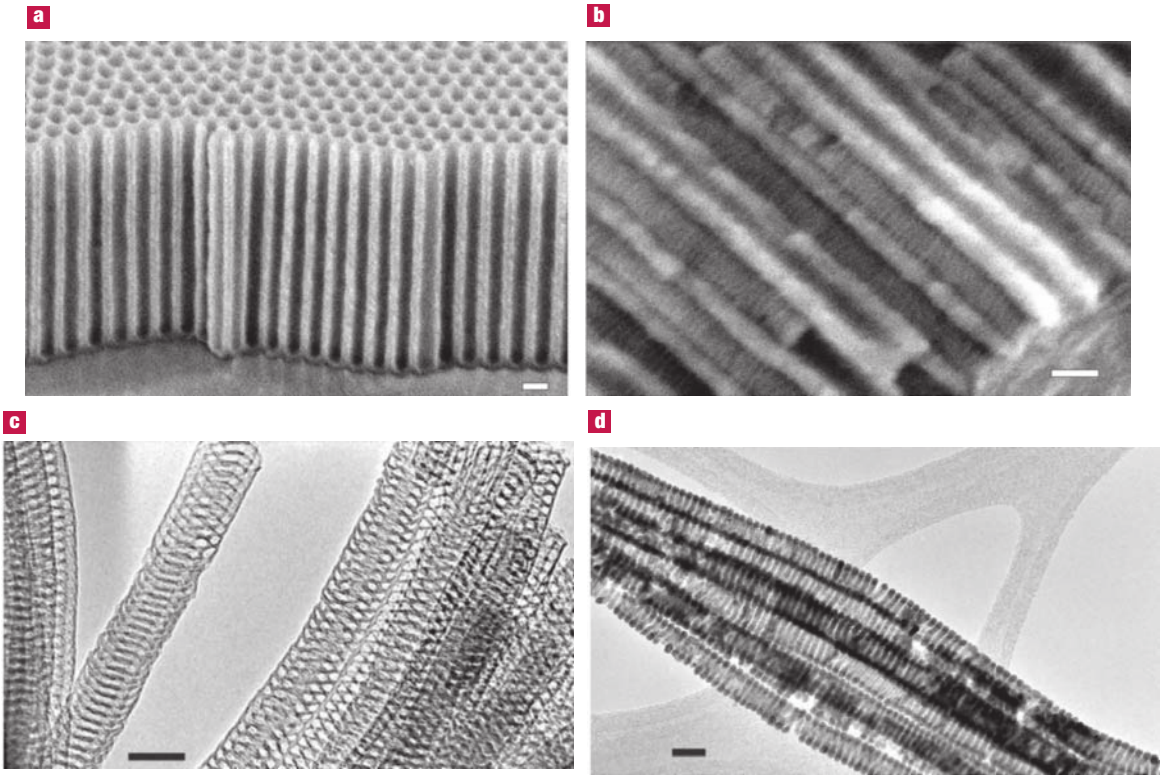

Figure 1 SEM images of PAA membrane and TEM images of free-standing mesoporous silica fibres and silver mesostructured nanowires. a, SEM image of the starting PAA membrane. **b**, SEM image of the PAA membrane cross-section after loading with mesoporous silica. **c**, TEM image of free-standing mesoporous silica fibres. **d**, TEM image of Ag nanowires with inverted mesostructures after their release from the oxide matrix. Scale bars: 100 nm in **a** and **b**, and 50 nm in **c** and **d**.

previously[13,14]. The alumina nanochannels acted, in essence, as a combinatorial nanoscale 'test tube' array in which the surfactant and the silica precursor molecules cooperatively assembled into specific mesostructures following the evaporation-induced self-assembly process[16]. The resulting mesostructured silica was calcined at 500 °C for 3 hours before further processing and analyses. Figure 1a and b shows scanning electron microscopy (SEM) images of the PAA membrane before and after loading with mesoporous silica.

The silica mesostructures formed inside the alumina channels were characterized by transmission electron microscopy (TEM). Samples were prepared in two ways: (1) the alumina matrix was dissolved by phosphoric acid to release the embedded mesoporous silica, which appeared as 1D nanofibres with ordered internal mesostructure (Fig. 1c); (2) 100-nm-thick slices were cut directly from the mesostructured-silica-loaded PAA membrane using a focused ion-beam system. To determine the 3D structure of the mesoporous nanofibres, a series of TEM images was taken at various tilting angles for the same nanofibre. As a comparison, simulated TEM images were calculated based on a presumed 3D mesostructure model. The agreement between the actual and simulated TEM images argues strongly for the accuracy of the presumed 3D model. Figure 2 shows an example with the triple-layered stacked-doughnut mesostructure. An important and complementary characterization approach is to backfill the voids of the confined mesoporous silica electrochemically with metals such as silver (Fig. 1d), producing inverted mesostructures[17].

The dip-coating precursor solution used here has previously been shown to form a 2D hexagonal SBA-15 mesostructured thin film on flat substrates with the long axes of the mesochannels oriented parallel to the substrate surface[13,14]. The effect of confinement can be thought to be equivalent to rolling up a flat substrate surface into a scroll and observing the effect on the mesostructures enclosed in the cylindrical space. A key question is whether the thin-film 2D hexagonal structure would be maintained, or whether the confinement effects might direct the molecular assembly to form new mesostructured composite configurations.

Figure 3 shows a series of TEM images of the mesostructures formed inside nanochannels of varying diameters. With nanochannel diameters ranging from 55 to 73 nm, the enclosed mesostructure is composed of three coaxial layers: a straight core channel and two outer layers consisting of concentric mesochannels with morphologies as diverse as stacked doughnuts, single helix (S-helix) or double helix (D-helix). Figure 3a shows an (inverted) three-layer Ag structure, in which the outer two layers are concentric stacked doughnuts spaced 13–14 nm apart. The diameter of the straight inner channel lies in the range 10–16 nm. Interestingly, if the Ag stacked-doughnuts structure is sonicated, it breaks up into individual nano-rings, indicating that the stacked doughnuts are loosely connected (see Supplementary Information, Fig. S1), and that their interconnectivity may, therefore, be similar to that of SBA-15 mesochannels with connecting micropores joining individual doughnuts[17]. Figure 3b shows the Ag inverted structure formed inside 64-nm-diameter alumina nanochannels, in which the outer layer has an S-helix structure with a pitch of 13 nm. In about 100 Ag mesostructured nanowires in this size range randomly chosen from the TEM images, ~35% are found to be stacked doughnuts, ~58% are S-helix and ~7% are D-helix.

When the alumina nanochannel diameter is reduced to 49–54 nm, the enclosed mesostructure becomes a coaxial double-layer helix in

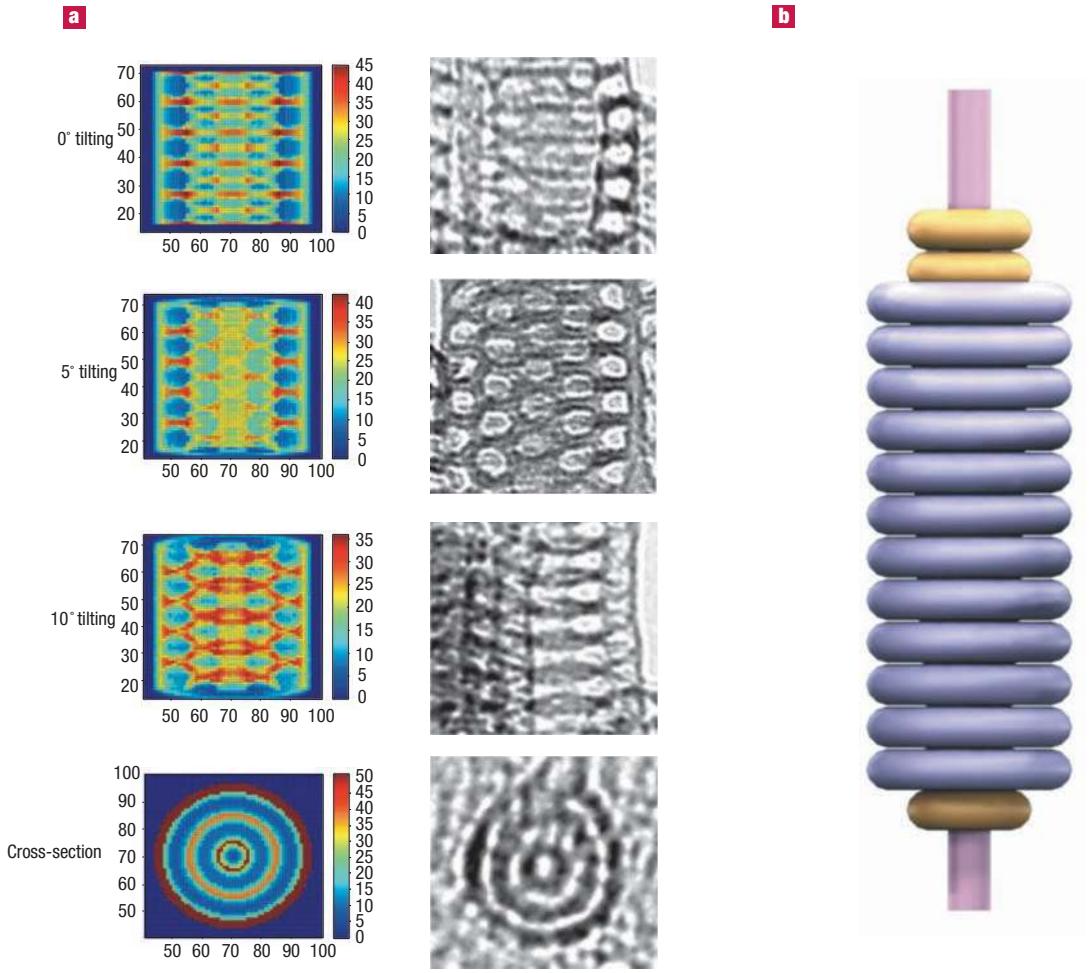

Figure 2 TEM image simulation and comparison with actual images of concentric three-layer stacked-doughnuts structure. a, TEM image simulation based on the concentric three-layer stacked-doughnuts structure at different electron incidence angles relative to the long axis of the mesostructured silica fibre (left frames) and the corresponding actual TEM images (right frames). The simulation results are presented as false-colour images with the colour index bars to the right side of the simulated images. The lower the colour index value in the simulated images (low values are blue, higher values red), the brighter the pixel of the actual TEM image. The tilting angle is defined as the angle between the electron incidence angle and the direction perpendicular to the long axis of the silica fibre. The diameter of the mesostructured silica fibre in the actual TEM images is 56 nm. **b**, Schematic model of the concentric three-layer stacked-doughnuts structure assumed in the TEM simulation.

which the inner core is an S-helix with a pitch of 30 nm and the outer layer is either an S-helix with a pitch of 13 nm (~80%) (Fig. 3c) or a D-helix with a pitch of 27 nm (~20%) (Fig. 3d). On further reducing the confinement dimension to 34–45 nm, the inner core becomes a straight channel with diameter in the range 13–16 nm and the outer layer consists either of stacked doughnuts (~50%), S-helix (~44%) or less-frequently D-helix (~6%) (Fig. 3e–g). Finally, with 31 nm nanochannels, the mesostructure becomes a single-layer D-helix with a 27 nm pitch (Fig. 3h).

With a confinement diameter below 30 nm, the helical architecture is no longer observed. Instead, a new mesopore morphology resembling an inverted peapod forms, composed of linearly packed spherical cages, which becomes two lines of spherical cages packed along the alumina nanochannel when the confinement dimension is reduced to 28 nm (Fig. 3i–j). Finally, when the confinement diameter becomes 18 nm, only a single line of aligned cages forms (Fig. 3k–l) with an average cage size of 14 nm.

Figure 4 summarizes the observed mesostructural evolution as a function of the cylinder confinement diameter. Viewed in this way, the 2D hexagonal-packed cylinder structure, which forms on a planar substrate, is the limiting case that would be observed when the diameter of the confining cylinder is infinite. The progression of observed morphologies leads to a simple structural scheme that connects the thin-film structure to the cylindrically confined doughnuts, S-helix and D-helix structures. All of these can be geometrically constructed by coiling up parallel cylinders using different rolling schemes (Fig. 5a–c). This paradigm provides a simple rationale of how changing the boundary symmetry (flat plane versus cylinder) induces the cylinder-forming mesophase to reorganize so as to fit in a cylindrical space of small dimension. Such a coiling strategy is also observed experimentally with lamella-forming precursor solutions, which form coaxial multilayered cylinder structures in hydrophilic alumina nanochannels (see Fig. 5d and Supplementary Information, Fig. S2). Among the various morphologies shown in Fig. 4, the formation of helical silica structures with chiral mesopores is of special interest, especially considering that the molecular organization processes do not make use of chiral molecules. These tightly coiled helical structures have

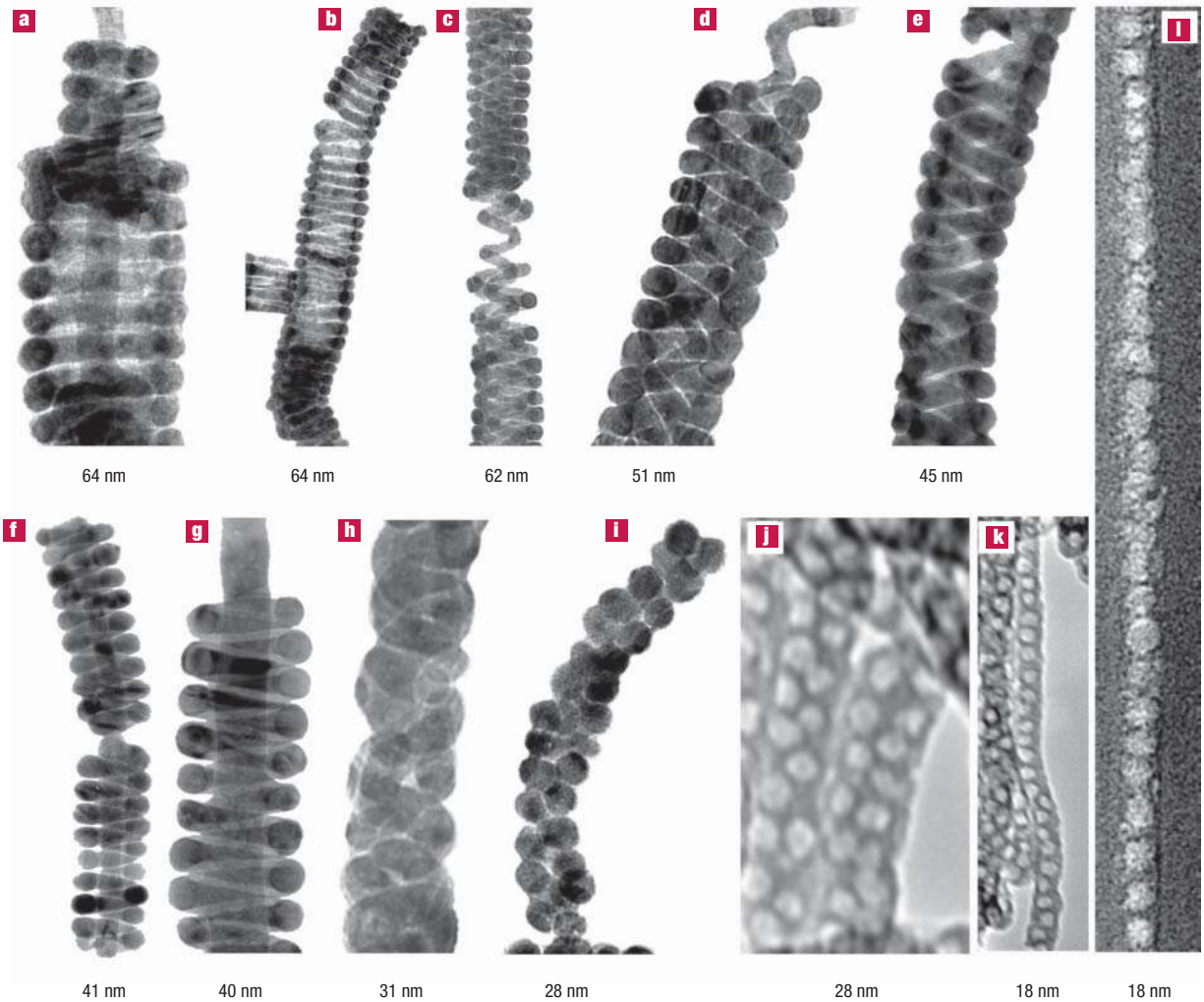

Figure 3 Representative TEM images of mesostructures formed inside alumina nanochannels with differing confinement dimensions. The confining nanochannel diameter is indicated underneath each image. **a**–**i**, Silver inverted mesostructures prepared by backfilling the confined mesoporous silica; **j**–**k**, free-standing mesoporous silica fibres; **l**, mesoporous silica embedded inside the alumina nanochannels obtained using a focused ion beam for sample preparation. The structures are **a**, three-layer stacked doughnuts; **b**, S-helix; **c**, core–shell D-helix, in which the core and the shell are both S-helix; **d**, core–shell triple-helix, in which the shell is a D-helix and the core is a S-helix; **e**, D-helix; **f**, **g**, S-helix with a straight core channel; **h**, D-helix; **i**, **j** inverted peapod structure with two lines of spherical cages packed along the long axis of the alumina nanochannel; **k**, **l**, inverted peapod with one line of cages.

no bulk counterparts and, to our knowledge, are unambiguously observed experimentally for the first time.

The coiling scheme also explains the observed 13 nm characteristic length in our work as the periodicity of the stacked doughnuts and the pitch of the S-helix structures. The architecture of stacked doughnuts and S-helix is geometrically constructed by the regular stacking of coiled cylindrical micelles and the spring-like curling of cylindrical micelles, respectively. The periodicity of the stacked doughnuts and the pitch of the S-helix should correlate with the inter-micelle spacing of the bulk mesophase. The 13 nm characteristic length scale in our work is in good agreement with the bulk SBA-15 lattice unit of 12 nm found previously[7] and the lattice spacing of bulk normal hexagonal lyotropic phase of P123–water (12 nm for ~50 wt% P123)[18].

Self-consistent field (SCF) calculations were carried out in an attempt to account for the observed self-assembled mesostructures. The SCF approach has been shown to be successful in describing both bulk and confined self-assembly of block-copolymer melts (see, for example, reviews[19,20]). In the bulk, the experimental amphiphile + solvent system closely resembles a diblock homopolymer blend in its behaviour: both systems form the same variety of mesophases as a function of solvent (homopolymer) volume fraction and temperature[19,21]. The interaction and structural parameters used in our SCF calculations were chosen to ensure only that the diblock copolymer + homopolymer blend forms the hexagonal phase in the bulk (see Methods). The mesostructures predicted by the simulation to arise under cylindrical confinement are shown in Fig. 6 (top row). The progression observed as the confinement diameter increases is as follows: spheres, to straight cylinder, to high-pitch helix or multi-helices, to the formation of a concentric inner shell. The trend is remarkably similar to what was observed experimentally. This leads us to conjecture that the confined mesostructures are universal in the same sense as the bulk behaviour referred to above.

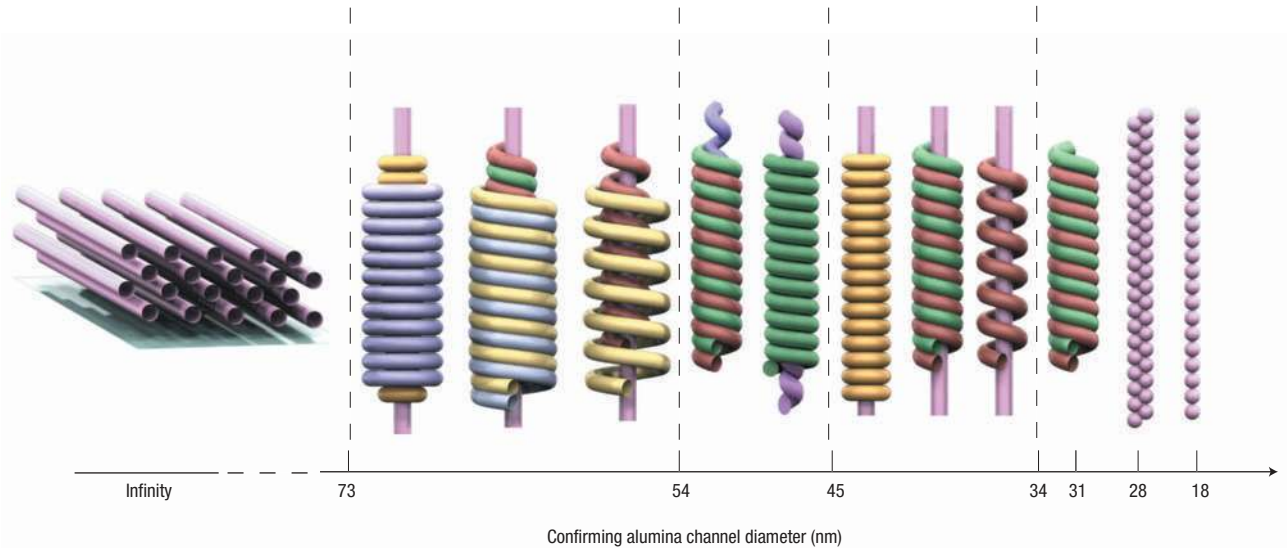

Figure 4 Summary of the experimentally observed confined mesostructural evolution with varying alumina nanochannel diameters.

The discrepancy in the long-range order between experiment and simulation suggests a 1D nucleation and growth mechanism. As water and ethanol evaporate, the large aspect ratio of the alumina pores can support a significant solvent concentration gradient in the axial direction. For a sufficiently small solvent concentration, the order–disorder transition is reached, thereby nucleating an effective '1D boundary' between the mesophase-separated and disordered phases. As solvent continues to evaporate, the confined mesophase propagates along the pore axis, producing the experimentally observed long-range order.

The confined silica–surfactant composite mesophases obtained here differ distinctly from those reported previously for confined polymer systems[22] in that the mesostructures obtained here form rigid silica frameworks that preserve their morphologies even after the surfactant is removed. This allows one to produce mesostructure arrays for a variety of possible applications. For example, PAA membranes loaded with silica–surfactant composite can be used to construct ultra-fine filters for size-dependent molecular separations[23]. The hierarchical pore configuration (silica mesopore confined within larger alumina nanochannels) improves the pore density and reduces the effective pore diameter. We measured the permeability through such membranes to illustrate this application (see Supplementary Information, Fig. S3). The effective membrane pore size and topography can be further tuned by choosing appropriate surfactants and precursor compositions[24,25]. The inner surface of mesoporous silica can also be grafted with various functional groups to improve the membranes' functionalities further (see Supplementary Information, Fig. S4). More interestingly, helical silica mesostructures with chiral mesopores could potentially be used for enantioselective separation provided that portions of the membrane can be found with helical pores of predominantly one chirality. The enantio-purity of the helical mesostructures (left-handed versus right-handed) and its control are currently under investigation.

Given the observed permeable nature of the confined silica mesostructures, they can also serve as templates for preparing

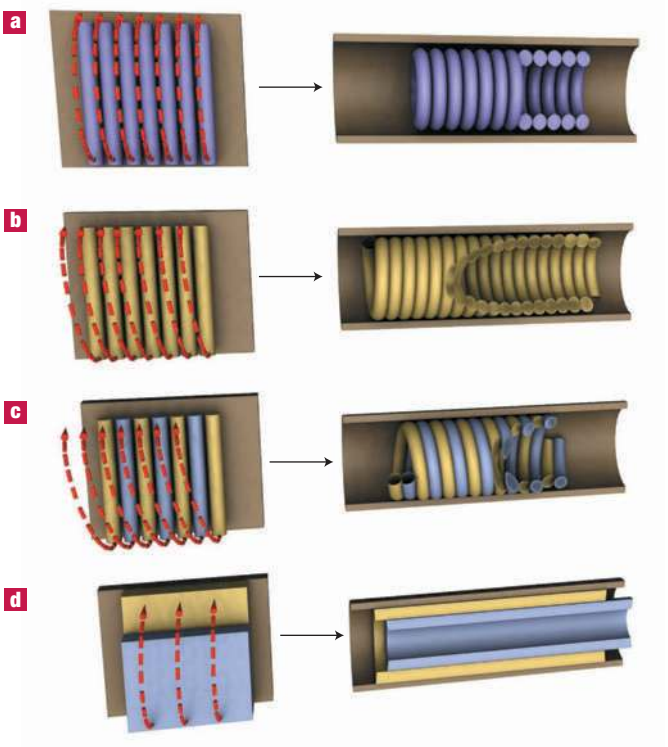

Figure 5 Schematic structural correlation between mesostructure formed on a flat substrate and that within a cylindrical confinement. The dotted red arrow indicates the direction of rolling the flat structure. **a–c**, Construction of stacked-doughnuts, S-helix and D-helix by rolling up the straight parallel mesochannels. When every mesochannel rolls back on itself to form a closed circle (**a**), the stacked-doughnuts structure forms. When the surface is rolled so that every mesochannel connects to the next mesochannel (**b**) or to the one after that (**c**) in the same layer, the S-helix and D-helix structures form, respectively. **d**, Rolling up lamella mesostructure parallel to the substrate results in a concentric multilayered cylinder structure.

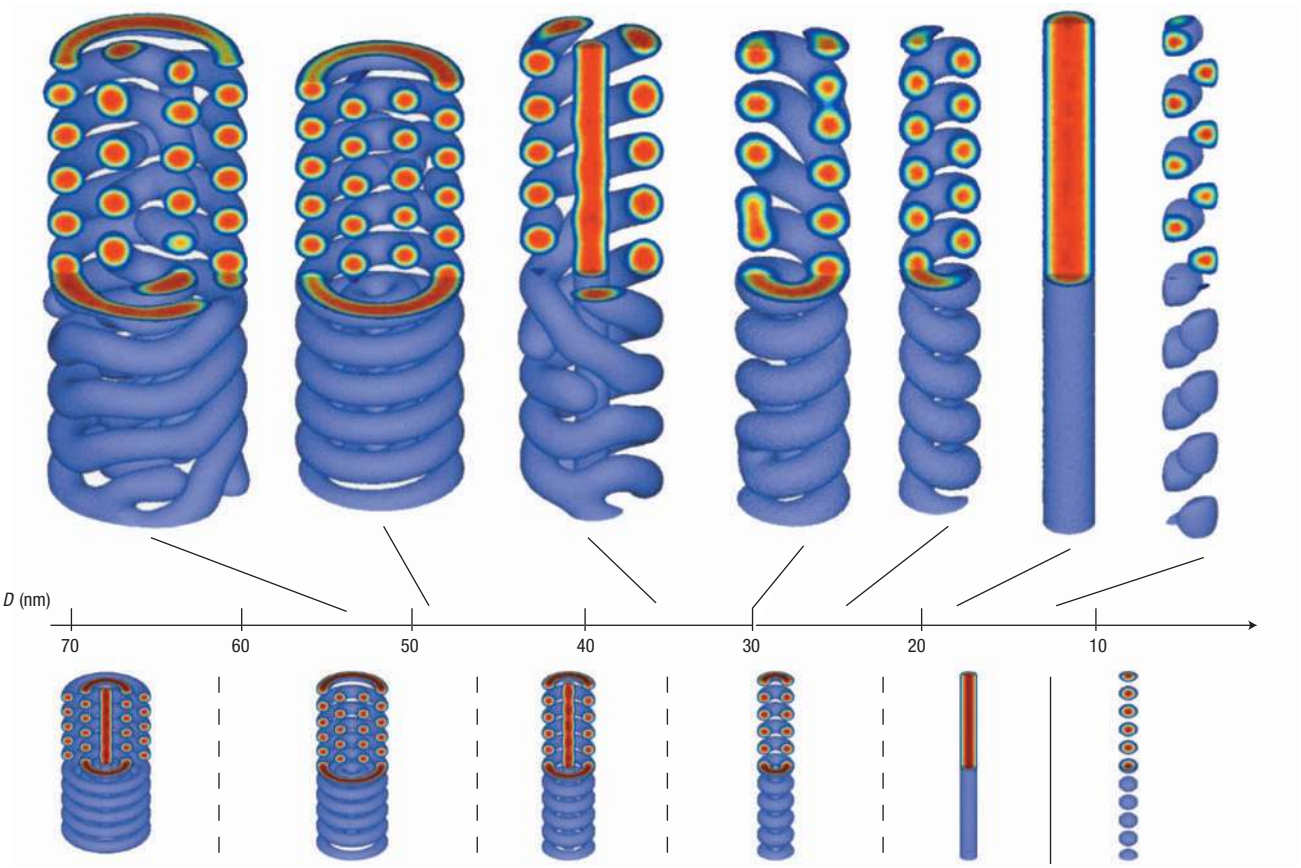

Figure 6 Simulated structures of the confined self-assembly in cylindrical confinement with varying cylinder diameter (*D*). Calculations were made using self-consistent field theory. Because some of the experimentally observed structures have axial symmetry, we also carried out calculations in cylindrical (*r*,*z*) coordinates (bottom row). The smaller dimensionality of the axially symmetric problem allowed us to study a wider range of the parameter space. In tight confinement, hexagonal packing of the cylindrical micelles running parallel to the pore axis would impose high stress on the system. This stress can be relieved by arranging the system into a set of concentric shells. In each shell the cylinders bend and tilt with respect to the pore axis, thus forming helices or doughnuts.

nanowires and nanowire arrays composed of a wide variety of mesostructured materials. This is illustrated by the electrochemically deposited Ag mesostructured nanowires shown in Figs 1d and 3a–i. Recent research on nanocrystals[26] and nanowires[27–29] has shown that the control of shape and structural complexity is important in defining the physical properties and functionalities of nanostructures. The structural features of the mesostructured nanowires obtained here are vastly different from solid nanowires in a variety of ways, including their periodically modulated surface morphology, high surface area, chirality (for helical nanowires) and hierarchical organization. These features have potential advantages for applications such as sensing, catalysis, thermoelectrics and opto-electronics. For example, highly regular silver mesostructured nanowires are appropriate for surface-enhanced Raman spectroscopy (see Supplementary Information, Fig. S5). The formation of D-helix and coaxially multilayered helical nanowires constitutes a wholly new architecture with subunits consisting of intertwined thinner nanowires, which would undoubtedly bestow unusual mechanical properties on the nanostructure. Moreover, electrochemical deposition can be used to deposit a very wide variety of materials (metals, semiconductors, oxides and polymers) in the mesoporous silica. In addition to Ag, we have also prepared Ni and Cu_2O mesostructured nanowires using these templates.

METHODS

PAA MEMBRANE PREPARATION

The PAA membrane was electrochemically fabricated on 0.14-mm-thick high-purity (99.999%) aluminium foil in 0.3 M oxalic acid using Masuda's two-step anodization process[11]. The anodization was carried out at 40 V d.c. at 15–17 °C. The second anodization step lasted 10 min, resulting in a nanochannel depth of 1.8–2 μm. For the samples that were used for electrochemical backfilling of Ag, a third anodization was carried out in 0.2 M H_3PO_4 for 10 min under the same conditions to reduce the thickness of barrier layer.

The nanochannels in the as-prepared PAA membrane are 28 ± 10 nm in diameter. They were controllably widened using 5 wt% H_3PO_4 to etch the PAA membrane further. For the diameter distribution at different etching times, see Supplementary Information, Fig. S6.

LOADING THE NANOCHANNELS WITH SILICA

The dip-coating precursor solution was prepared as follows: to pre-hydrolysed tetraethyl orthosilicate (TEOS) in diluted hydrochloric acid (pH 2) and ethanol solution, we added poly (ethylene oxide)-*b*-poly (propylene oxide)-*b*-poly (ethylene oxide) block copolymer $EO_{20}PO_{70}EO_{20}$ (Pluronic P123), which was initially dissolved in ethanol. The mixture was stirred for 3 hours. The final molar ratio of the precursor solution was 1 TEOS: 0.0096 P123: 6 H_2O: 8.8 ethanol: 0.001 HCl for the 2D hexagonal cylinder mesostructure (SBA-15)[13,14]. The lamella-forming precursor solution had 0.36 times as much TEOS[14]

The precursor solution was loaded into PAA nanochannels by dip-coating (at a speed of 12 cm min^{-1}). The loaded PAA membrane was subsequently aged at 25 °C and a relative humidity of 65–70% for 24 hours. It was then calcined at 500 °C for 3 hours. That temperature was reached at a ramp rate of 1 °C min^{-1}. For further quality control and consistency, a glass slide was dip-coated immediately after every PAA membrane and went through the same subsequent treatments. The silica thin film on the glass slides consistently showed 2D hexagonal and lamella structure in X-ray diffraction pattern at low angles for cylinder-forming and lamella-forming precursor solutions, respectively (see Supplementary Information, Fig. S7).

CHARACTERIZATION OF EMBEDDED SILICA MESOSTRUCTURES

TEM samples were prepared in two ways: (1) a focused ion-beam system (FEI DB235 duel-beam) was used to cut a 100-nm-thick slice out of the silica-loaded PAA membrane, which was subsequently transferred to a TEM sample grid using a micro-manipulator; and (2) the PAA membrane was completely dissolved in 5 wt% H_3PO_4 releasing the mesostructured silica from its PAA host followed by transfer to a TEM grid.

The backfilling of Ag was carried out by electrochemical deposition in a solution of 0.05 M $AgNO_3$ and 0.5 M H_3BO_4 at 28 V a.c. and 200 Hz. For TEM characterization, the Ag inverted structures were released from the oxide matrix by etching in 0.1 M NaOH. We used FEI Tecnai G2 Sphera microscope operated at 200 kV for TEM imaging.

Other characterization tools such as grazing-incidence 2D small-angle X-ray scattering were also used (see Supplementary Information, Fig. S8).

SELF-CONSISTENT FIELD THEORY CALCULATIONS

Self-consistent field theory (SCFT) for dense polymer melts is a method whereby the hamiltonian of a complex system is transformed into a coarse-grained field theory description, whose mean-field solution is amenable to a wide array of analytical and numerical methods. We solve the SCFT equations using a numerical algorithm[30,31] that does not require any information about the equilibrium morphologies. This numerical method is flexible and has great predictive capability; however, it is computationally intensive and requires large memory resources. The 3D results in Fig. 4 (top row) were obtained by implementing the numerical SCFT algorithm on a massively parallel MPI computer cluster[32].

The polymer chains are modelled by a hamiltonian that includes free-energy contributions due to the stretching of the chains and the interaction energy between the chemically distinct A/B monomers forming the diblocks and the C monomers on the homopolymer chains. These interaction energies are parameterized by the quantities χ_{AB}, χ_{BC} and χ_{AC} in a Flory-type model. The 3D results shown in Fig. 4 were obtained from simulations of a diblock copolymer + homopolymer blend system with $\chi_{AB} = \chi_{BC} = 0.15$ and $\chi_{AC} = 0.001$. The length of the homopolymer chains is half the length of the diblocks, the hompolymer chains occupy 30% of the total volume of the pore interior, and 60% of each diblock chain consists of A monomers. The pore walls attract C monomers while repelling A and B monomers.

Received 29 July 2004; accepted 18 August 2004; published 17 October 2004.

References

1. Kellogg, G. J. *et al.* Observed surface energy effects in confined diblock copolymers. *Phys. Rev. Lett.* **76,** 2503–2506 (1996).
2. Chen, H. Y. & Fredrickson, G. H. Morphologies of ABC triblock copolymer thin films. *J. Chem. Phys.* **116,** 1137–1146 (2002).
3. Lambooy, P. *et al.* Observed frustration in confined block-copolymers. *Phys. Rev. Lett.* **72,** 2899–2902 (1994).
4. Zhu, S. *et al.* Confinement-induced miscibility in polymer blends. *Nature* **400,** 49–51 (1999).
5. Sevink, G. J. A., Zvelindovsky, A. V., Fraaije, J. G. E. M. & Huinink, H. P. Morphology of symmetric block copolymer in a cylindrical pore. *J. Chem. Phys.* **115,** 8226–8230 (2001).
6. Zhao, D. Y., Huo, Q. S., Feng, J. L., Chmelka, B. F. & Stucky, G. D. Nonionic triblock and star diblock copolymer and oligomeric surfactant syntheses of highly ordered, hydrothermally stable, mesoporous silica structures. *J. Am. Chem. Soc.* **120,** 6024–6036 (1998).
7. Zhao, D. Y. *et al.* Triblock copolymer syntheses of mesoporous silica with periodic 50 to 300 angstrom pores. *Science* **279,** 548–552 (1998).
8. Ying, J. Y., Mehnert, C. P. & Wong, M. S. Synthesis and applications of supramolecular-templated mesoporous materials. *Angew. Chem. Int. Edn* **38,** 56–77 (1999).
9. Tsai, C. Y., Tam, S. Y., Lu, Y. F. & Brinker, C. J. Dual-layer asymmetric microporous silica membranes. J. *Membrane Sci.* **169,** 255–268 (2000).
10. Yang, P. D. *et al.* Mirrorless lasing from mesostructured waveguides patterned by soft lithography. *Science* **287,** 465–467 (2000).
11. Masuda, H. & Satoh, M. Fabrication of gold nanodot array using anodic porous alumina as an evaporation mask. *Jpn J. Appl. Phys.* **35,** L126–L129 (1996).
12. Lu, Y. F. *et al.* Continuous formation of supported cubic and hexagonal mesoporous films by sol–gel dip-coating. *Nature* **389,** 364–368 (1997).
13. Zhao, D. *et al.* Continuous mesoporous silica films with highly ordered large pore structures. *Adv. Mater.* **10,** 1380–1385 (1998).
14. Alberius, P. C. A. *et al.* General predictive syntheses of cubic, hexagonal, and lamellar silica and titania mesostructured thin films. *Chem. Mater.* **14,** 3284–3294 (2002).
15. Crepaldi, E. L. *et al.* Controlled formation of highly organized mesoporous titania thin films: From mesostructured hybrids to mesoporous nanoanatase TiO_2. *J. Am. Chem. Soc.* **125,** 9770–9786 (2003).
16. Brinker, C. J., Lu, Y. F., Sellinger, A. & Fan, H. Y. Evaporation-induced self-assembly: nanostructures made easy. *Adv. Mater.* **11,** 579–585 (1999).
17. Joo, S. H., Ryoo, R., Kruk, M. & Jaroniec, M. Evidence for general nature of pore interconnectivity in 2-dimensional hexagonal mesoporous silicas prepared using block copolymer templates. *J. Phys. Chem. B* **106,** 4640–4646 (2002).
18. Holmqvist, P., Alexandridis, P. & Lindman, B. Modification of the microstructure in block copolymer–water–'oil' systems by varying the copolymer composition and the 'oil' type: Small-angle X-ray scattering and deuterium-NMR investigation. *J. Phys. Chem. B* **102,** 1149–1158 (1998).
19. Matsen, M. W. Phase-behavior of block-copolymer homopolymer blends. *Macromolecules* **28,** 5765–5773 (1995).
20. Schmid, F. Self-consistent-field theories for complex fluids. *J. Phys. Condensed Matter* **10,** 8105–8138 (1998).
21. Janert, P. K. & Schick, M. Phase behavior of binary homopolymer/diblock blends: Temperature and chain length dependence. *Macromolecules* **31,** 1109–1113 (1998).
22. Fasolka, M. J. & Mayes, A. M. Block copolymer thin films: Physics and applications. *Annu. Rev. Mater. Res.* **31,** 323–355 (2001).
23. Jirage, K. B., Hulteen, J. C. & Martin, C. R. Nanotubule-based molecular-filtration membranes. *Science* **278,** 655–658 (1997).
24. Yamaguchi, A. *et al.* Self-assembly of a silica-surfactant nanocomposite in a porous alumina membrane. *Nature Mater.* **3,** 337–341 (2004).
25. Lu, Q. Y., Gao, F., Komarneni, S. & Mallouk, T. E. Ordered SBA-15 nanorod arrays inside a porous alumina membrane. *J. Am. Chem. Soc.* **126,** 8650–8651 (2004).
26. Manna, L., Milliron, D. J., Meisel, A., Scher, E. C. & Alivisatos, A. P. Controlled growth of tetrapod-branched inorganic nanocrystals. *Nature Mater.* **2,** 382–385 (2003).
27. Wu, Y. Y., Fan, R. & Yang, P. D. Block-by-block growth of single-crystalline Si/SiGe superlattice nanowires. *Nano Lett.* **2,** 83–86 (2002).
28. Bjork, M. T. *et al.* One-dimensional steeplechase for electrons realized. *Nano Lett.* **2,** 87–89 (2002).
29. Gudiksen, M. S., Lauhon, L. J., Wang, J., Smith, D. C. & Lieber, C. M. Growth of nanowire superlattice structures for nanoscale photonics and electronics. *Nature* **415,** 617–620 (2002).
30. Maurits, N. M. & Fraaije, J. G. E. M. Mesoscopic dynamics of copolymer melts: From density dynamics to external potential dynamics using nonlocal kinetic coupling. *J. Chem. Phys.* **107,** 5879–5889 (1997).
31. Fredrickson, G. H., Ganesan, V. & Drolet, F. Field-theoretic computer simulation methods for polymers and complex fluids. *Macromolecules* **35,** 16–39 (2002).
32. Sides, S. W. & Fredrickson, G. H. Parallel algorithm for numerical self-consistent field theory simulations of block copolymer structure. *Polymer* **44,** 5859–5866 (2003).

Acknowledgements

This work was supported by the National Science Foundation under award number DMR 01-20967 and award number DMR 02-33728, and partially supported by the MRSEC Program of the National Science Foundation under award no. DMR 00-80034 and by an IBM Faculty Award. We thank R. C. Hayward and T. Livneh for helpful discussions.

Correspondence and requests for materials should be addressed to G.D.S.

Supplementary Information accompanies the paper on www.nature.com/naturematerials

Competing financial interests

The authors declare that they have no competing financial interests.